Global and Planetary Change 118 (2014) 42–51

Contents lists available at ScienceDirect

Global and Planetary Change

journal homepage: www.elsevier.com/locate/gloplacha

A study of the longest tide gauge sea-level record in Greenland (Nuuk/Godthab, 1958–2002)

G. Spada [a,*], G. Galassi [a], M. Olivieri [b]

[a] Dip.to di Scienze di Base e Fondamenti, Università di Urbino, Urbino, Italy
[b] Istituto Nazionale di Geofisica e Vulcanologia, Sezione di Bologna, Italy

ARTICLE INFO

Article history:
Received 20 January 2014
Received in revised form 3 April 2014
Accepted 7 April 2014
Available online 16 April 2014

Keywords:
Sea-level change
Tide gauge observations
Greenland ice sheet

ABSTRACT

We study the longest tide gauge record available from Greenland, that is the Nuuk/Godthab site in southwest Greenland, for the time period 1958–2002. Standard regression methods and the application of the Ensemble Empirical Mode Decomposition technique reveal a rate of sea-level rise of ≈ 2 mm yr^{-1}, two complete cycles of the 18.6-years lunar nodal tide, and a negligible acceleration. Using previous assessments for the globally averaged sea-level rise during that period, glacial isostatic adjustment modeling and sea-level "fingerprinting" of the mass loss of continental ice sources, terrestrial water sources and oceanic steric effects, we evaluate the various contributions to local sea-level rise at the tide gauge location. The misfit between the observed and the modeled sea-level trend is unlikely to reflect tectonic deformations but, more intriguingly, may indicate that the mass balance of the Greenland ice sheets was, during the second half of the last century, somehow closer to balance than suggested by previous investigations.

1. Introduction

Since the seminal work of Gutenberg (1941), observations from tide gauges deployed along the world's shorelines have been recognized as a fundamental tool for the study of the global mean sea-level rise (for a review, see Spada and Galassi, 2012). The long term tide gauge records reflect various processes that change the total mass of the oceans (mass term) or their density in response to thermal expansion and salinity variations (steric component). The mass term includes effects from the melting of continental ice sheets, glaciers and ice caps, the alteration of land water reservoirs, and hydrological variations originating from human activity (see e.g., Milne et al., 2009; Cazenave and Remy, 2011).

Although the number and the quality of tide gauges observations have dramatically increased since the birth of the Permanent Service for Mean Sea Level (PSMSL) in 1933 (Woodworth and Player, 2003; Holgate et al., 2012), their geographical distribution remains largely non-uniform and biased toward the northern hemisphere. As of today, only a few tens of time series have a sufficient length for an assessment of secular sea-level variations (Douglas, 1991, 1997; Spada and Galassi, 2012) (only 73 PSMSL annual records have a length exceeding 100 years). In addition, they require suitable corrections for the effects of sediment compaction, water or hydrocarbon extraction, tectonics, and glacial isostatic adjustment (GIA). However, at the present time, global models useful for computing such corrections only exist for GIA (Spada and Galassi, 2012). Recent estimates of global mean sea-level rise point to values in the range between 1.5 and 2 mm yr^{-1}, although a significant scatter still exists, reflecting different approaches and averaging methods applied (Spada and Galassi, 2012).

In view of rapid changes affecting the polar ice sheets (see the Intergovernmental Panel on Climate Change (IPCC) Fourth Assessment Report, hereinafter AR4, Bindoff et al., 2007), in situ sea-level observations from these regions would be potentially very important. In particular, it is expected that relative sea-level observations from tide gauges located in the vicinity of major ice sheets could help to constrain the recent time-history of their mass unbalance (before the year ~2000, this was only poorly determined because of the limited resolution of remote sensing techniques, see Bindoff et al., 2007). However, despite significant collaborative efforts, at the end of the nineties the state of polar tide gauges was generally unsatisfactory. The whole subject was reviewed by Plag (2000), who pointed out the degradation of the observing system and emphasized the relevance of Arctic tide gauge data for the geophysical community. Nonetheless, in some specific locations, such as southwest Greenland, the sparsity of instrumental observations can be partly alleviated using data from salt marshes (Woodroffe and Long, 2009), which are potentially valuable for reconstructing the relative sea-level variations during the last few centuries (Barlow et al., 2013).

As of the year 2000, a small number of tide gauges were in operation along the Arctic shores of Russia, Greenland, Iceland, Norway, Canada and USA (Plag, 2000). Among these, a few were characterized by record lengths exceeding a few decades, and thus are potentially suitable for estimating local long-term sea-level trends. For Norway and Russia,

* Corresponding author.
E-mail address: giorgio.spada@gmail.com (G. Spada).

http://dx.doi.org/10.1016/j.gloplacha.2014.04.001
0921-8181/

the state of the tide gauges has been recently reviewed by Henry et al. (2011), who have highlighted the importance of these observations for the assessment of the mass and steric components of recent sea-level rise. However, the situation was, and still remains, particularly problematic in Greenland, where the PSMSL database now collects records from only eight sites (Fig. 1), mostly located along the southwest margins of the Greenland ice sheet (GIS). The instrumental record from the Nuuk/Godthab tide gauge, hereafter referred to as NG, is remarkably long (>40 years) compared to other sites in Greenland (≤10 years), and covers a time span ~1958–2003 during which only a few assessments of the GIS mass balance are available (Hanna et al., 2005; Bindoff et al., 2007; Rignot et al., 2008; Slangen, 2012). The PSMSL tide gauge time series for Greenland are visualized in Fig. 2, which also shows the length (P, years) and completeness (c,%) of each record.

The context above encourages a new analysis of the NG record, which aims to test the consistency of the NG datum with the various contributions to sea-level rise in southwest Greenland and, in particular, to ascertain whether relative sea-level data from this site could be useful for constraining volume changes in the GIS during the second half of last century. We extend the previous analysis of Plag (2000), who recognized that trends shown by Arctic tide gauges are in broad agreement with an overall un-loading of the Arctic land-based cryosphere, and by Fleming et al. (2009) who focused on the present-day GIA contributions to sea-level change around Greenland. However, in comparison with previous studies, here we consider a longer time frame and we perform a more detailed study taking advantage of the AR4 assessments, of numerical modeling based on the solution of the "Sea Level Equation" (Farrell and Clark, 1976), and of the computation of sea-level "fingerprints" (Mitrovica et al., 2001; Tamisiea et al., 2011). Although we focus on an individual tide gauge record, our approach could be extended to other Arctic records with sufficient lengths.

The paper is organized as follows: in Section 2 we analyze the NG time series, in Section 3 we examine various contributions to sea-level change at NG, and we discuss the results in Section 4, with the conclusions presented in Section 5.

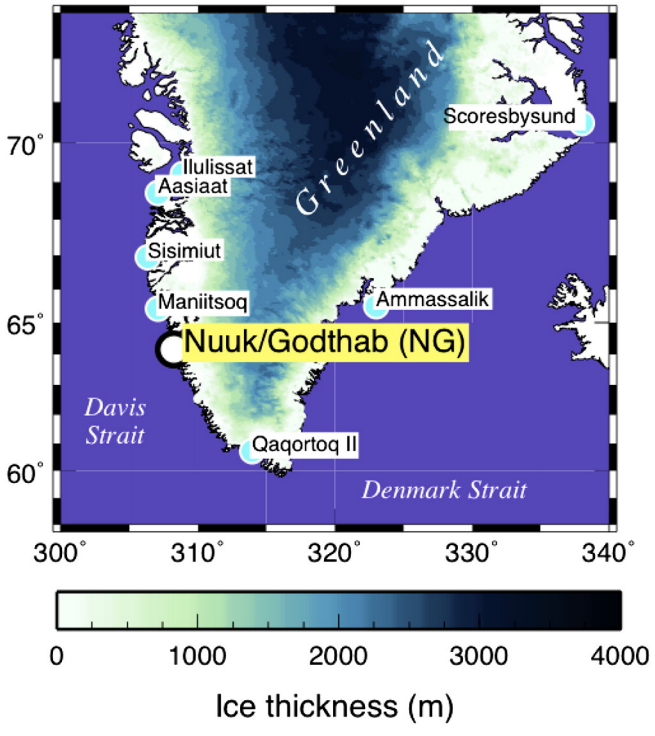

Fig. 1. Map of southern Greenland, showing the location of the Nuuk/Godthab (NG) tide gauge (longitude = 51.73°W, latitude = 64.17°N) and of other PSMSL sites in Greenland: Ilulissat, Aasiaat, Sisimiut, Maniitsoq, Qaqortoq II, Ammassalik and Scoresbysund. The time series for these tide gauges are displayed in Fig. 2. The figure also shows the present-day ice thickness of the GIS (in meters); ice thickness data are from Bamber et al. (2013).

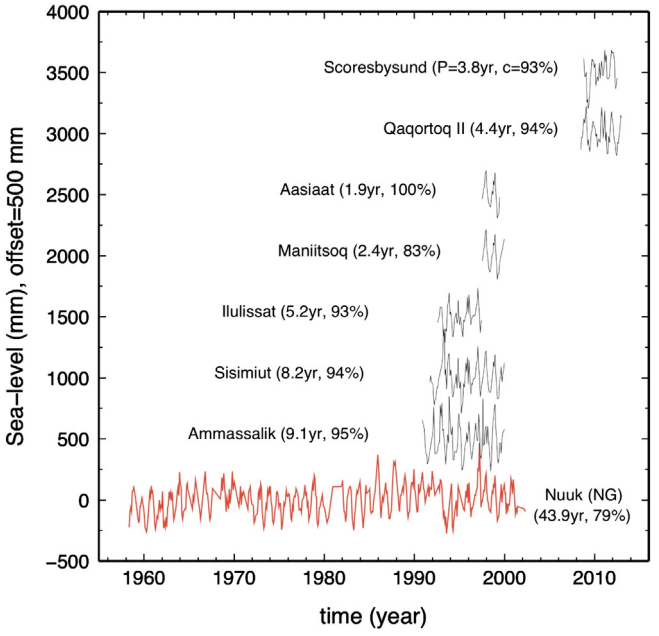

Fig. 2. Overview of the PSMSL metric monthly time series available from the Greenland sites in Fig. 1. For visualization purposes, the time series have been shifted by 500 mm and the average has been subtracted. The record length P (in years) and the completeness c (%) are also shown.

2. Sealevel trend at the NG tide gauge

The NG tide gauge record, obtained from the database of the PSMSL (http://www.psmsl.org/[1]), contains monthly mean sea-level values between 1958.4 and 2002.3. The total time span of the record is thus P = 43.9 years and its completeness is c = 79% (the minimum completeness requested by Douglas (1997) and Spada and Galassi (2012) in their studies on secular sea-level rise was c = 80% and 70%, respectively). The time series does not belong to the RLR ("Revised Local Reference") PSMSL dataset; rather, the data is from the "metric" dataset, hence the benchmark is arbitrary and jumps are undetected (unfortunately, only metric observations are available from Greenland). Nevertheless, the NG observations can be used in this context, since we are mostly interested in the average rate of relative sea-level rise over several decades, which is unaffected by the choice of the benchmark. In 2002, the NG instrument was damaged and is no longer maintained by the DMI (Danish Meteorological Institute). Coincidentally, the time period of the NG tide gauge almost exactly overlaps the one adopted in the AR4 assessments of the total budget of global mean sea-level change during the second part of the 20th century (namely, 1961–2003). In her recent study, Slangen (2012) also payed specific attention to this time period. This will greatly facilitate, in Section 3, comparisons between the observed rate at the NG site and existing assessments for the various components of sea-level change.

The NG time series is reproduced in Fig. 3a. A few interruptions are visible, which, however, do not affect seriously its completeness. Although a small change of coordinates is reported in 1969 in the PSMSL station documentation, a visual inspection does not reveal anomalies or discontinuities in the record at that epoch. Since Nuuk is located along the western coast of Greenland (see Fig. 1), distant from collisional boundaries, tectonic deformations are not expected to significantly contaminate the observations. The NG time series suggests the

[1] Extracted from Database 26 June 2013.

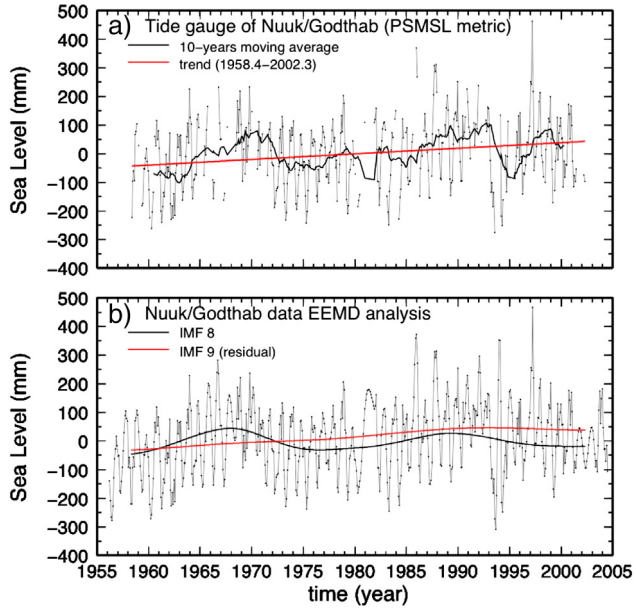

Fig. 3. (a): The NG time series (thin dotted curve are where segments join consecutive monthly values, while isolated points imply interruptions in the time series), its 10-year moving-average (thick black curve), and the linear trend over the whole observation period (red line) obtained by least squares. (b): Interpolated and mirrored NG record (thin dotted curve), the Intrinsic Model Function IMF8 corresponding to the longest period (~18 years) in the EEMD analysis (black curve), and the residual (red). (For interpretation of the references to color in this figure legend, the reader is referred to the web version of this article.)

existence of a long-term linear trend and of large amplitude oscillations with a period of ~2 decades, which are likely to represent the effects of the 18.6 years nodal tide (Trupin and Wahr, 1990). The oscillations are particularly evident after the application of a 10-year running average (thick line in Fig. 3a), clearly showing that the nodal tide attains almost exactly two full cycles within the time window of the NG data. Therefore, it is expected that the assessment of the trend is not too biased by this oscillating component of the signal.

To estimate the local long term sea-level trend from the NG data, we first performed a straight-forward linear regression. Considering the whole time period of the NG record (1958.4–2002.3), the inferred rate of sea-level change is $(+1.9 \pm 0.7)$ mm yr^{-1}, where the uncertainty has been evaluated by the explicit expressions given by Spada and Galassi (2012) and corresponds to the 95% confidence interval. The trend is shown by a red line in Fig. 3a. The sea-level acceleration (twice the quadratic term of a second order polynomial regression) for the NG time series is (-0.05 ± 0.04) mm yr^{-2}. By a Fisher F-test performed on the variances of the residues of the linear and quadratic regressions, we have verified that the latter does not improve the fit with respect to the former at the 95% confidence level.

In contrast to a simple regression, the Empirical Mode Decomposition (EMD) technique does not require a-priori assumptions about the functional expression of the regression model (Huang et al., 1998). Furthermore, it is particularly suitable for analyzing non-linear and non-stationary time series (Barnhart, 2011). In this method, time series are split into a finite set of empirically orthogonal Intrinsic Mode Functions (IMFs) describing cyclic variations not necessarily characterized by constant amplitudes and phases. The EMD is thus particularly useful for isolating the terms with dominating periodicities from a tide gauge record. After the subtraction of the IMFs, the residual reveals the "natural" trend of the signal, which is not constrained to have a predetermined polynomial form.

Here we use an improved version of the EMD method (the "ensemble EMD", or EEMD, see Wu and Huang, 2009), namely the Complete Ensemble Empirical Mode Decomposition with Adaptive Noise (CEEMDAN), described by Torres et al. (2011) and implemented in MATLAB.[2] The EEMD has been recently employed by Breaker and Ruzmaikin (2013) to study the long-term trend of the San Francisco tide gauge record. The method requires the estimate of two parameters. The first (Nstd) determines the noise level, and is defined as the ratio of the standard deviation of the first IMF (IMF1) to the standard deviation of the original time series. For the NG record, the value obtained is Nstd = 0.30. The second parameter (NE) defines the number of realizations required to construct IMFs; in this case, following Breaker and Ruzmaikin (2013), we use NE = 300. Since the EEMD method is adaptive, the number of IMFs is not set a-priori, but is determined by the data themselves.

Since the EEMD requires continuous data, gaps in the original NG time series have been filled by a cubic spline interpolation (De Boor, 1978). In addition, following Qingjie et al. (2010), errors due to end effects are prevented by applying a mirroring technique. In Fig. 3b, we show the NG time series after interpolation and mirroring, the residual (red curve) obtained after subtracting the IMFs, and the IMF8 (black curve) which represents the oscillation with the longest period (~18 years). To obtain a linear trend from the residual, we have performed a standard linear regression, which provides a rate of (1.93 ± 0.03) mm yr^{-1}. Adding in quadrature the uncertainty in the residual itself, we obtain

$$r^{OBS} = +1.93 \pm 0.18 \quad \text{mm yr}^{-1}, \tag{1}$$

(95% confidence), for the time period 1958.4–2002.3 (extrapolating our assessment to the time interval 1961–2003, the same considered in the AR4, does not significantly change the estimate). While the value obtained is consistent with the one gained above by a standard linear regression, the strong improvement in its precision results from the removal of the cyclic components implied in the EEMD approach. Note that in Eq. (1) and in the following, the uncertainty will be expressed using two significant figures, even when the fractional uncertainty is large. This is generally contrary to common practice (see e.g., Taylor, 1997), but it facilitates comparison with the AR4 results.

The value of r^{OBS} in Eq. (1) is comparable with the average rate of global sea-level change during the period 1961–2002 ($+1.8 \pm 0.8$ mm yr^{-1}, where the uncertainty denotes the 95% confidence interval) assessed by AR4. According to Table 3 of Wahl et al. (2013), these values are also in broad agreement with the rate of global sea-level rise during 1950–2009 (namely, 1.80 ± 0.11 mm yr^{-1}), and with the regional rate for the North Sea (1.62 ± 0.29 mm yr^{-1}) during the same period. However, in view of the large local effects expected at the NG tide gauge from GIA and in particular from the isostatic effects associated with the melting of the nearby GIS, this agreement is certainly fortuitous.

3. Sea-level components at the NG tide gauge

The long-term rate of relative sea-level change observed at tide gauges stems from the combination of several components. Following the general approach outlined by Slangen (2012) and Spada and Galassi (2012), this can be tentatively written as:

$$r^{OBS} = r^{GIA} + r^{STE} + r^{MAS} + r^{TEC} + r^{OTH}, \tag{2}$$

where the observed rate r^{OBS} is constrained by Eq. (1), r^{GIA} is the GIA component of sea-level change (associated with the response of the Earth following the last deglaciation, 21–4 kyrs BP), r^{STE} is the steric component arising from changes in the ocean's temperature, r^{MAS} is the contribution associated with mass exchange (referred to as the "mass term" in the following), and terms r^{TEC} and r^{OTH} account for the contribution of tectonic movements and of other possibly unknown factors, respectively (the latter including, for instance, sediments

[2] See: http://bioingenieria.edu.ar/grupos/ldnlys/metorres/re_inter.htm.

compaction and anthropogenic effects). In turn, the mass term in (2) can be modeled as:

$$r^{MAS} = r^{TER} + r^{AIS} + r^{GIC} + r^{GIS}, \tag{3}$$

where the terms on the right hand side are associated with terrestrial water mass exchange, including impoundment by dams and groundwater mining (r^{TER}), and mass variations of the Antarctic Ice Sheet (r^{AIS}), glaciers and ice caps (r^{GIC}), and of the Greenland ice sheet (r^{GIS}), respectively. The Inverse Barometer correction has been neglected here, since its globally averaged value during 1961–2003 is <0.1 mm yr^{-1}, its signature is mainly meridional, and southern Greenland is sited close to the zero contour line of this sea-level component (see Fig. 3.2e of Slangen, 2012).

Some of the terms of Eqs. (2) and (3) are individually discussed in the following subsections, with reference to the NG tide gauge. A possible role for the tectonic component will be addressed in Section 4.

3.1. The GIA component

Fig. 4a and b show the sea-level fingerprints associated with GIA at global and regional scales, respectively. Since the time scale of GIA is of the order of a few kilo-years (Turcotte and Schubert, 2002), the rates of sea-level change shown in Fig. 4 can be considered to be constant over the time period of concern here (a few decades). The maps are obtained by adopting the model ICE-5G(VM2) of Peltier (2004), based on an extension of the gravitationally self-consistent sea-level theory first proposed by Farrell and Clark (1976). Gridded solutions of the "Sea Level Equation" (SLE) for model ICE-5G(VM2) have been downloaded from the home page of W.R. Peltier on August 2013. Since for this model the ice sheets' melting ends ~4000 years ago, GIA is not currently causing any alterations in the total mass of the oceans, but is of course producing regional sea-level variations due to the Earth's on-going adjustment to the changes following the LGM (Last Glacial Maximum). As a consequence, for the fingerprints in Fig. 4, the average sea-level (ASL) is

$$\left\langle r^{GIA} \right\rangle = 0, \tag{4}$$

where here and in the following, the symbol $\langle \cdots \rangle$ denotes the average over the surface of the oceans. However, this property does not hold for the mass terms in Eq. (3) since, in contrast with GIA, they currently involve a net mass variation of the oceans, as well as surface displacements due to local changes.

Across the Davis Strait (i.e., between Greenland and Canada, see Fig. 4b), a sea-level rise of several millimeters per year results from the combined effects of two processes, namely the collapse of the isostatic forebulge surrounding the former Laurentian ice sheet and the melting of the Greenland ice sheet. The relative contributions of these two processes have been separately studied by Fleming and Lambeck (2004). The rate of sea-level rise is strongly reduced along the coasts of southwest Greenland and it changes its sign to the south. According to the current version of model ICE-5G(VM2), the rate of GIA-induced sea-level change at the NG tide gauge is

$$r^{GIA}_{ICE-5G(VM2)} = +0.67 \quad \text{mm yr}^{-1}, \tag{5}$$

with an unspecified uncertainty (for NG and all the other PSMSL tide gauges, numerical predictions for sea-level change are available from http://www.atmosp.physics.utoronto.ca/peltier/). In view of the large gradients of GIA-induced sea-level variations in southwest Greenland shown in Fig. 4b, we expect that details in the GIA modeling assumptions, both in terms of the ice mass descriptions and Earth rheology used, could lead to significantly different results.

To estimate the uncertainty associated with r^{GIA}, we have carried two further GIA runs (R1 and R2) in which two different global chronologies for the melting history of the late-Pleistocene ice sheets have been employed (the computations have been made using an improved version of the program SELEN by Spada and Stocchi, 2007). The chronologies are ICE-5G and the one progressively developed at the Research School of Earth Sciences (RSES) of the National Australian University by Kurt Lambeck and co-workers (see Lambeck et al., 1998 and references therein). Since the latter is valid as of 2005, it will be referred to as KL05 in the following (Kurt Lambeck, personal communication, 2012). ICE-5G and KL05 differ significantly for the global distribution of the ice masses, and in particular for the post Last Glacial Maximum GIS chronologies, and are constrained by different relative sea-level datasets. As pointed out by Spada et al. (2012), these differences have a significant impact on predictions of present-day vertical uplift along the coast of Greenland.

The results of the two runs are shown in Fig. 5. For run R1, we have employed a three layer viscosity profile for the mantle, obtained by volume-averaging the multi-layered VM2 profile of Peltier (2004). The upper mantle, transition zone, and lower mantle Maxwell viscosities are 0.5, 0.5 and 2.7 × 10^{21} Pa·s, respectively, and the lithospheric thickness is 90 km. For run R2, we have adopted the nominal viscosity profile of Fleming and Lambeck (2004), which is constrained by Holocene relative sea-level observations in Greenland. In this case, the upper mantle, transition zone, and lower mantle viscosities are 0.4, 0.4 and

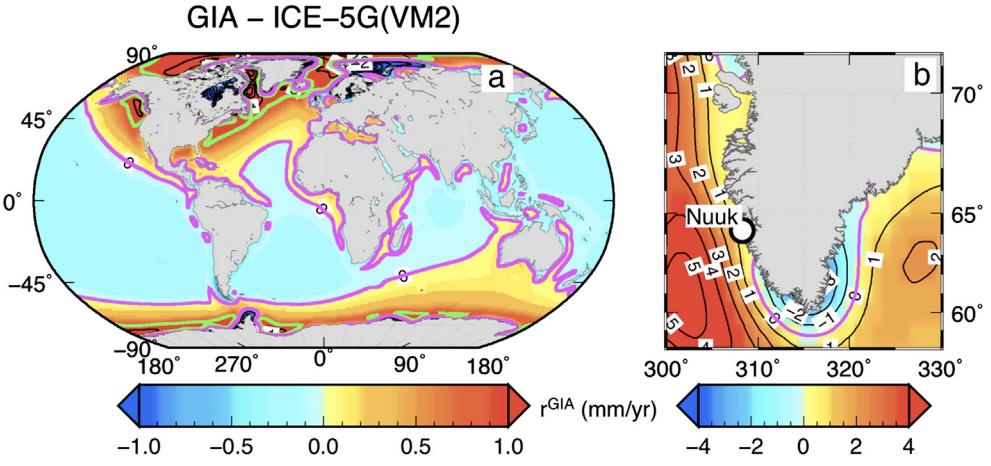

Fig. 4. (a): Global view of r^{GIA}, the rate of present-day sea-level change due to GIA from the Last Glacial Maximum (21 ka) (r^{GIA}), obtained using model ICE-5G(VM2) (Peltier, 2004). The magenta and the green contours mark the particular values $r^{GIA} = 0$ and $r^{GIA} = 1$ mm yr^{-1}, respectively. (b): Detail of (a) showing a regional-scale contour plot of r^{GIA} for southern Greenland. (For interpretation of the references to color in this figure legend, the reader is referred to the web version of this article.)

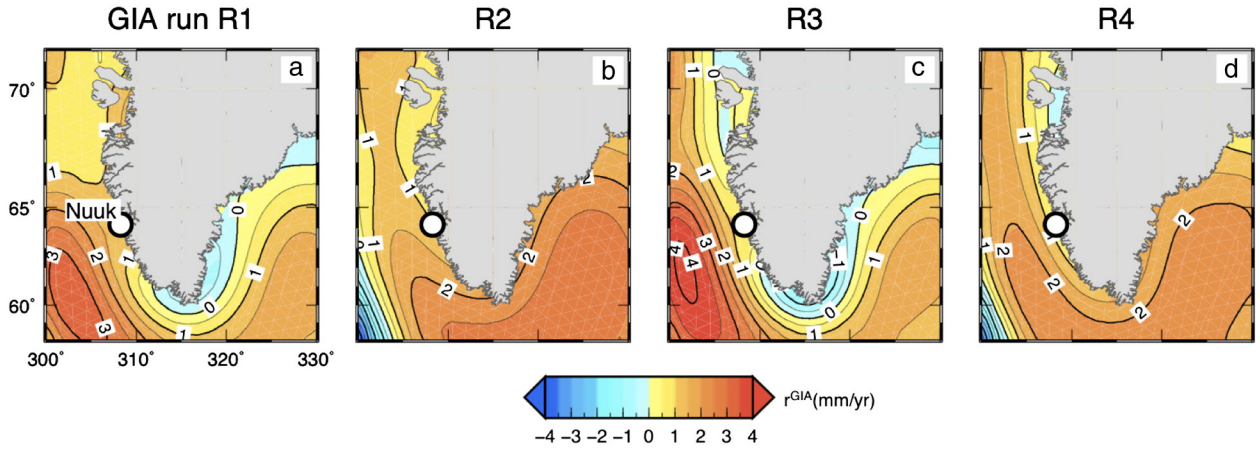

Fig. 5. (a): Regional sea-level variations in southern Greenland according to four distinct GIA models. Models ICE-5G and KL05 are employed in runs (R1, R3) and (R2, R4), respectively. The mantle is incompressible in (R1, R2) and compressible in (R3, R3). Details about the modeling are given in Section 3.1. (For interpretation of the references to color in this figure legend, the reader is referred to the web version of this article.)

10×10^{21} Pa·s, respectively, with a lithospheric thickness of 80 km. We did not vary these viscosity values, since this would alter the match of the GIA model predictions with the Holocene relative sea-level variations used to constrain their parameters. The formulation by Milne and Mitrovica (1998) has been employed to account for the impact of Earth rotation variations on sea-level change. Runs R1 and R2 have in turn been repeated adopting the recipe by Tanaka et al. (2011) in order to mimic the effects of mantle compressibility, and the results are shown in Fig. 5 as GIA runs R3 and R4, respectively. Despite the significant spatial variability shown by the GIA response in southwest Greenland (see Fig. 5), in all the computations performed, the GIA-induced rate of sea-level change tends to decrease close to the shorelines.

The values of GIA-induced sea-level rise predicted at the NG site are 1.54, 1.03, 0.81, and 0.64 mm yr^{-1}, for models R1, R2, R3 and R4, respectively. Along with the value corresponding to the nominal ICE-5G(VM2) model (Eq. (5)), these values define the interval

$$r^{GIA} = +1.1 \pm 0.5 \text{ mm yr}^{-1}, \quad (6)$$

which represents our preferred estimate for the current rate of GIA-induced sea-level change at NG. From Fig. 5, we note that the spread of the GIA predictions is sensibly larger along the eastern coasts of Greenland.

A comparison of (6) with (1) indicates that GIA is one of the dominating terms in Eq. (2); however, the effective role of GIA can be assessed only by evaluating all the other contributions. We note that according to recent assessments of the GIS during the last decade (see e.g., Sørensen et al., 2011), which imply uplift rates of ~3 mm yr^{-1} in southwest Greenland (Spada et al., 2012), the relative importance of GIA is now greatly reduced in this region.

3.2. The thermosteric component

Bindoff et al. (2007) have evaluated the ocean-average steric component to total sea-level rise during two distinct time periods: 1961–2003 and 1993–2003. Their assessments are presented in Table 5.3 of the AR4. For the former period, which almost exactly overlaps the time span of the NG tide gauge record, they provide an ASL of

$$\left\langle r^{STE}_{AR4} \right\rangle = +0.42 \pm 0.12 \text{ mm yr}^{-1}, \quad (7)$$

(90% confidence), while during the latter there is evidence of a significant increase in the steric component, with values close to 1.5 mm yr^{-1}. Estimate (7), which accounts for thermal expansion to a depth of 3000 m, combines results from Antonov et al. (2005) and Ishii et al. (2006).

The geographical distribution of linear trends in thermal expansion for the period 1955 to 2003 is highly non-uniform, especially across the equatorial oceans (see Fig. 5.16 of the AR4, based on Ishii et al., 2006). From a visual inspection of this figure, in the Davis Strait the trend of the thermosteric component of sea-level change was positive during that time period, with values possibly below the global average (Eq. (7)). To obtain a more refined estimate of the total steric component of sea-level rise at Nuuk, we have analyzed the data available from the National Oceanographic Data Center (NODC), see http://www.nodc.noaa.gov/. In particular, we have considered fields of the steric sea-level anomaly down to a depth of 2000 m, during the time period between the pentads 1958–1962 and 2000–2005. The regional pattern of the average rate for southwest Greenland is displayed in Fig. 6. Using values from ocean pixels within the 3° × 3° area marked by a

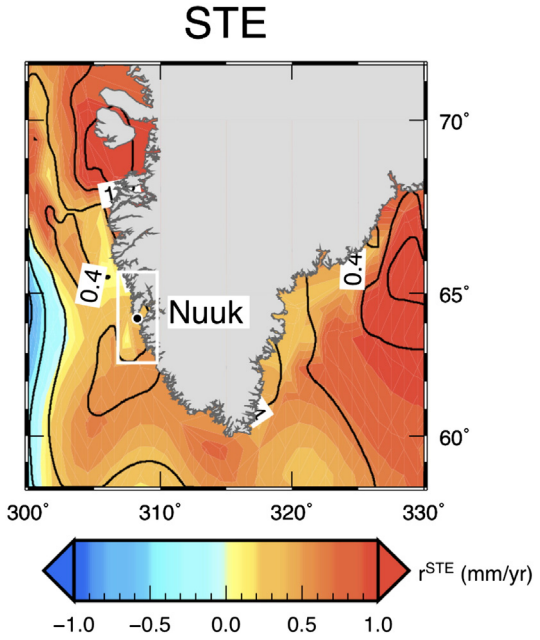

Fig. 6. Steric component of sea-level change in southern Greenland between 1958–1962 and 2000–2005 according to the NODC data. The 3° × 3° rectangle surrounding NG contains the ocean pixels that have been used to obtain the estimate of r^{STE} given in Eq. (8).

rectangle in Fig. 6, we obtain

$$r^{STE} = +0.39 \pm 0.14 \ \text{mm yr}^{-1}, \quad (8)$$

where the uncertainty represents the standard deviation of the mean. This overlaps with the estimate (7) based on the AR4 report. Using steric anomalies to a depth of 700 m, also available from the NODC, would not change appreciably the value of r^{STE} in the area surrounding Nuuk. We note that Eq. (8) does not account for possible bottom pressure variations caused by ocean warming and circulation changes. However, using a coupled Atmosphere-Ocean General Circulation Model under the IPCC-A1B scenario, Landerer et al. (2007) have shown that these will play a role, especially in shelf areas, during the 21st and 22nd centuries.

3.3. The TER component

The terrestrial exchange (TER) sea-level fingerprint for the time period 1961–2003 (Fig. 7) mostly shows negative values. It has been constructed by Slangen (2012), combining groundwater extraction data from Wada et al. (2012) and reservoir impoundment data from Chao et al. (2008). The two processes contribute to produce a sea-level fall and a total ocean-averaged effect of

$$\left\langle r^{TER} \right\rangle = -0.20 \pm 0.20 \ \text{mm yr}^{-1}, \quad (9)$$

where the uncertainty has been estimated by adding in quadrature the individual uncertainties of the contributing mechanisms (see Table 3.1 of Slangen, 2012). In the region of the Davis Strait, the TER component of sea-level rise is

$$r^{TER} = -0.07 \pm 0.07 \ \text{mm yr}^{-1}, \quad (10)$$

which therefore represents the smallest mass term in Eq. (3).

3.4. The AIS component

For the mass term AIS in Eq. (3), the ASL assessed by AR4 is

$$\left\langle r^{AIS}_{AR4} \right\rangle = +0.14 \pm 0.41 \ \text{mm yr}^{-1}, \quad (11)$$

during the period 1961–2003 (again, see Table 5.3 of Bindoff et al., 2007). As discussed in greater detail in Section 4, this is simply a reasonable estimate, since no supporting data effectively exist for the mass balance of the AIS during this period of time.

Since the NG tide gauge is located in the extreme far-field of Antarctica, Eq. (11) is expected to constitute a valid approximation for the rate of local sea-level change. In fact, a property of the sea-level fingerprints is that at very large distances from the ice source, a value greater than the ocean-averaged value is reached, largely a result of the direct gravitational response (Mitrovica et al., 2001). This is confirmed by the results presented in Fig. 8, where Fig. 8a shows the global (normalized) sea-level fingerprint (i.e., the ratio $r/\langle r \rangle$) corresponding to the melting of the AIS, while Fig. 8b shows its regional pattern. These have been obtained by solving the SLE using SELEN under the assumption of an elastic rheology for the mantle, which is appropriate in view of the short time scale considered here (a few decades), compared to those of GIA. A uniform net mass variation over the AIS is also assumed. In view of the axial symmetry of the AIS, the global fingerprint shows little effect from the rotational feedback on sea-level (Mitrovica et al., 2001). However, larger effects are expected for the GIC and the GIS.

Using the AR4 assessment in Eq. (11) and the numerical values presented in Fig. 8b, our estimate for the AIS component of total sea-level change at NG is

$$r^{AIS} \simeq +1.1 \left\langle r^{AIS}_{AR4} \right\rangle = +0.15 \pm 0.45 \ \text{mm yr}^{-1}. \quad (12)$$

3.5. The GIC component

To evaluate the mass term r^{GIC} in Eq. (3), we have solved the SLE employing the distribution of mountain glaciers and ice caps tabulated by Meier (1984), assuming a uniform net mass variation over the sources. The corresponding global normalized sea-level fingerprint is shown in Fig. 8c. In comparison with the AIS and GIS (this latter is considered in Section 3.6 below), the GIC fingerprints show a larger spatial variability, which reflects the scattered distribution of the GIC sources.

The site of NG (Fig. 8d) is located very close to the nodal line of the sea-level fingerprint, corresponding to a minimal sea-level change. This is consistent with the results obtained by Mitrovica et al. (2001) (see their Fig. 1c), even though they did not assume a uniform mass variation across the GIC. The same is found in Slangen (2012). From the numerical results presented in Fig. 8d, we obtain:

$$r^{GIC} \simeq +0.25 \left\langle r^{GIC}_{AR4} \right\rangle = +0.13 \pm 0.05 \ \text{mm yr}^{-1}, \quad (13)$$

while

$$\left\langle r^{GIC}_{AR4} \right\rangle = +0.50 \pm 0.18 \ \text{mm yr}^{-1} \quad (14)$$

represents the ASL assessed by the AR4 for the period 1961–2003, essentially based on the work of Dyurgerov and Meier (2005). This value includes glaciers and ice caps around major ice sheets and its uncertainty corresponds to the 90% confidence interval. The large

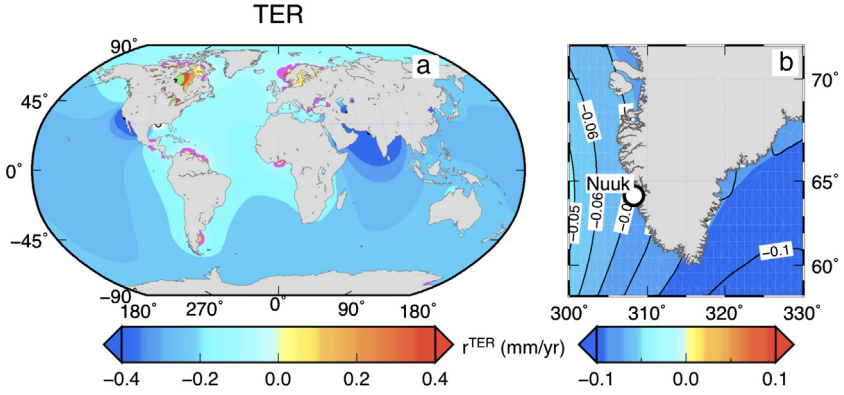

Fig. 7. Global (a) and regional (b) views of the mass term r^{TER} of sea-level change for the time period 1961–2003. The magenta and the green contours have the same meaning as in Fig. 4. The gridded data for this figure have been provided by Aimee Slangen (personal communication, 2013). (For interpretation of the references to color in this figure legend, the reader is referred to the web version of this article.)

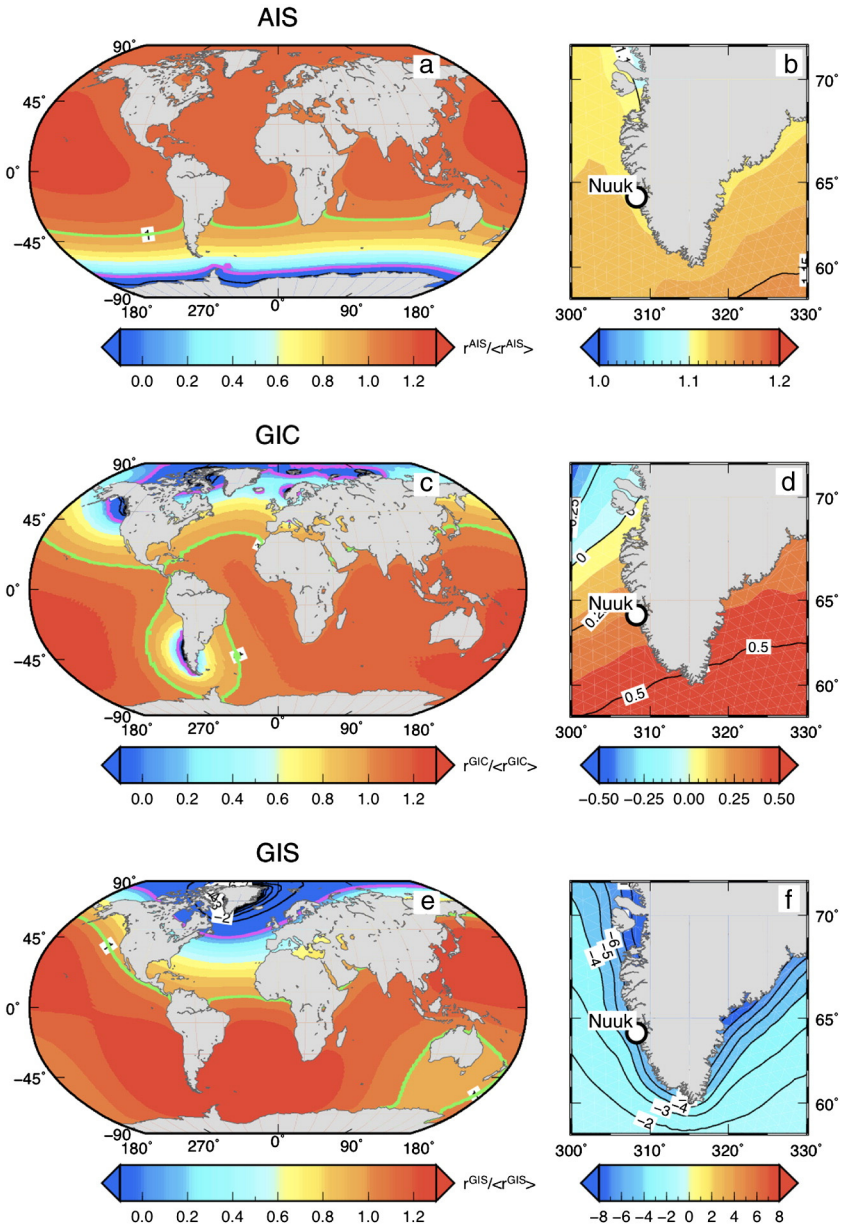

Fig. 8. Normalized sea-level fingerprints ($r/\langle r\rangle$) for the AIS (top), GIC (middle) and GIS (bottom), where r is the rate of relative sea-level change and $\langle r\rangle$ is its ocean-average. The contours with $r/\langle r\rangle = 0$ and $r/\langle r\rangle = 1$ are marked in magenta and green, respectively. Different color tables are employed for the global (left) and regional maps (right) for ease of assessment. (For interpretation of the references to color in this figure legend, the reader is referred to the web version of this article.)

discrepancy of r^{GIC} from the globally averaged value is the consequence of the relatively small distance separating the NG tide gauge from the major GIC sources in the northern polar region.

3.6. The GIS component

The GIS sea-level fingerprint is shown in Fig. 8e and f. Since we do not dispose of a detailed mass balance for the GIS during the time period 1961–2003, these fingerprints have been obtained assuming a uniform mass variation over the GIS, as we have done for the GIC and the AIS components in previous sections. On a global scale (8e), this is characterized by a pattern of far-field sea-level rise, in excess of the eustatic average $\langle r^{GIS}\rangle$, as seen for the AIS, and by broad swathes in the southern Atlantic and eastern Pacific oceans associated with the rotational effects on sea-level change (Mitrovica et al., 2001). In contrast to the AIS and GIC results, the regional GIS sea-level fingerprint (8f) is markedly characterized by negative values, caused by the uplift of the solid Earth in response to the ice mass loss as well as the decreased gravitational attraction of the nearby ice sheet (see Spada et al., 2012).

For the rate of ASL rise caused by the GIS melting during the period 1961–2003, three estimates are available, none of which are based on the NG tide gauge datum. While they are overlapping, since they are not fully equivalent, they will be considered separately in the following. The first, published by AR4, is

$$\left\langle r^{GIS}_{AR4}\right\rangle = +0.05 \pm 0.12 \ \text{mm yr}^{-1}, \tag{15}$$

which is largely based on Hanna et al. (2005), but also accounts for other mass balance estimates obtained for the period 1993–2003 (see Fig. 4.18 of the AR4). Since $\langle r^{GIS}_{AR4}\rangle$ results from a very small number of assessments, its uncertainty has not a statistically rigorous significance and it does not correspond to a specific confidence level. We note that within the range of uncertainty, $\langle r^{GIS}_{AR4}\rangle$ also includes negative values

that would correspond to a positive mass balance for the GIS (ice mass accretion) during the period 1961–2003.

After the publication of the AR4, the work of Hanna et al. (2005) was extended and updated by Rignot et al. (2008). By averaging the total mass balance estimates given in their Fig. 3 over the time period 1960–2000, a second estimate for the ASL rise can be obtained

$$\left\langle r^{GIS}_{R08} \right\rangle = +0.20 \pm 0.08 \quad \text{mm yr}^{-1}, \tag{16}$$

which suggests a larger contribution of the GIS compared to (15).

A third estimate has been recently given by Slangen (2012), who combined surface mass balance data from Ettema et al. (2009) with the dynamical component of ice loss from Rignot et al. (2011), suggesting:

$$\left\langle r^{GIS}_{S12} \right\rangle = +0.14 \pm 0.16 \quad \text{mm yr}^{-1}, \tag{17}$$

which only marginally includes negative values, indicative of an increase of the GIS mass.

Taken all together, estimates (15), (16) and (17) point to an ASL rise $\langle r^{GIS} \rangle$ in the range between +0.1 and +0.2 mm yr^{-1}. From the normalized-fingerprint values in Fig. 8f, one has

$$r^{GIS} \simeq -5.5 \left\langle r^{GIS} \right\rangle, \tag{18}$$

which allows for a straightforward computation of the local rate of sea-level rise expected at the NG tide gauge during 1961–2003 according to the three estimates above for $\langle r^{GIS} \rangle$. Note that, in (18), the large scaling factor in front of $\langle r^{GIS} \rangle$ denotes the large departure from eustasy arising from NG being in the near-field of the GIS.

Various results, reviewed by Alley et al. (2010), strongly indicate that during last decade, $\langle r^{GIS} \rangle$ has increased considerably above the values reported for the period 1961–2003, implying a significant acceleration (Velicogna, 2009; Rignot et al., 2011). In particular, according to the recent ICESat-based estimate of Sørensen et al. (2011) and Spada et al. (2012), the ASL rise associated with the melting of the GIS has been $\langle r^{GIS} \rangle = 0.67 \pm 0.08$ mm yr^{-1} between 2003 and 2008, exceeding by one order of magnitude the AR4 assessment for 1961–2003 (15).

4. Discussion

In Fig. 9, the top lines (black) summarize the numerical values obtained F9 in Section 3 for the various sea-level change contributions (Eqs. (2) and (3)). While the GIA term is only obtained from modeling, the others are based on various assessments given in the literature. For the mass terms, estimates of local sea-level variations have been obtained by modeling. Concerning the GIS, three rates are given, corresponding to three different estimates for the average sea-level change given in Section 3.6. It is apparent that the GIA and the GIS terms provide the largest contribution to sea-level variation at NG during period 1961–2003. The two terms, however, are counteracting, with the GIA producing a relative sea-level rise and the changes in the GIS having the tendency to produce a sea-level fall, according to the three estimates considered here. The remaining mass terms (AIS, GIC and TER) have a minor role, and, in general, are characterized by a large fractional uncertainty. However, together with the STE term, they act in the same direction as the GIA term (i.e., sea-level rise). The three MOD lines in Fig. 9 (blue) show the total modeled and/or assessed values for the rate of sea-level change at NG. They result from adding the terms of lines 1.–5. with each of the three GIS contributions corresponding to the estimates of AR4, of Rignot et al. (2008) (R08) and of Slangen (2012) (S12), respectively.

Although the fractional uncertainties in the MOD values are relatively large, a comparison with the observed rate (red in Fig. 9) is possible, at least qualitatively. All the MOD rates indicate positive rates of sea-level change, as seen in the observed trend. The observed trend is fully consistent (the error bars completely overlap) with the model predictions based on the AR4 assessment for the GIS component, while the agreement is only marginal if we consider the MOD value based on the Slangen (2012) estimate. The observed rate is clearly inconsistent with the MOD rate inferred from the Rignot et al. (2008) results. Overall, the results in Fig. 9 indicate that the level of the disagreement between the rate of sea-level change inferred from NG and the predictions resulting from modeling or obtained from the literature is of the order of 0.5–1 mm yr^{-1}, which represents a significant fraction of the observed rate.

The general misfit between the observations and model predictions in Fig. 9 could be attributed to an erroneous evaluation of one or more of the terms in Eq. (2) or to some unmodeled effects. Since the GIA and the GIS have the largest amplitudes, errors in the evaluations of these two terms would be the most likely contribution to the disagreement. In particular, the assumption of a uniform mass balance for the GIS maybe the source of significant errors. Due to the very low urbanization in the Nuuk region, anthropogenic effects can safely be excluded. Systematic errors associated with the instrumentation, however, cannot be ruled out. Another possible source of misfit could, in principle, be associated with tectonic deformations associated with the r^{TEC} term in

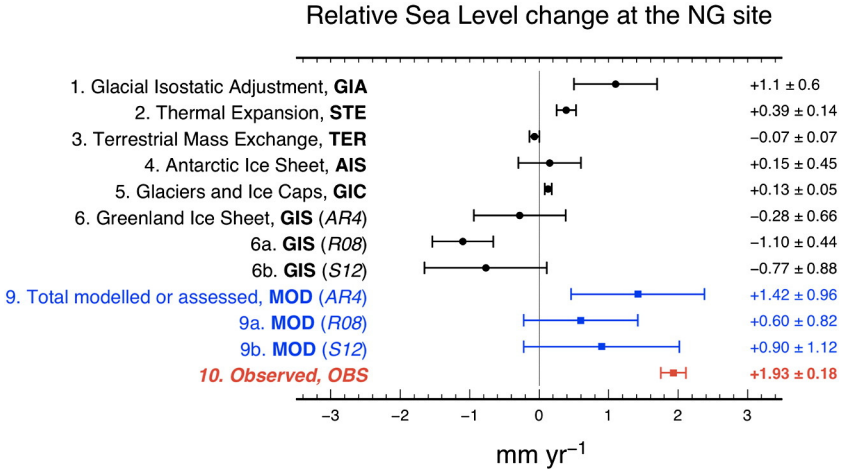

Fig. 9. Summary of individual modeled (or assessed) contributions to the sea-level trend expected at the NG tide gauge during the period 1961–2003 (black), the total modeled or assessed sea-level change (MOD, blue) and the observed trend (OBS, red) at the NG tide gauge. The error bars on the total MOD rates are obtained by adding in quadrature the individual (independent) uncertainties of the individual sea-level contributions. Note that for the GIS, three estimates are available, and thus three MOD rates. Numerical values are given in the right-hand column. (For interpretation of the references to color in this figure legend, the reader is referred to the web version of this article.)

Eq. (2). These have been often invoked as a possible cause of long-term sea-level variations at tide gauges (Spada and Galassi, 2012; Olivieri et al., in press). Previous work (e.g., Chung and Gao, 1997) has suggested that Greenland is a tectonically stable region with a low level of seismicity (Johnston, 1987) possibly controlled by on-going GIA (Chung, 2002). Furthermore, observations of vertical rates of crustal uplift observed by Global Positioning System (GPS) along the coasts of Greenland can be satisfactorily explained, at least during 2003–2008, by combining GIA effects based on the ICE-5G model of Peltier (2004) with isostatic deformations associated with the present-day elastic response to ice unloading, without invoking tectonic deformations (Spada et al., 2012). Although the agreement between predictions of isostatic models and GPS vertical rates is particularly good at the GPS site of KELY in southwest Greenland, relatively close to the location of the NG tide gauge, a role for tectonic subsidence cannot be ruled out at the 0.5 mm yr^{-1} level, since the uncertainty on the longest GPS vertical rates is still above the 1 mm yr^{-1} level (see Table 3 of Spada et al., 2012). Possible effects from the vertical deformations associated with cryospheric fluctuations during the Little Ice Age (LIA) are expected to produce small effects in SW Greenland, even assuming an extremely low asthenospheric viscosity (Valentina Barletta, personal communication, 2013).

Assuming that the trend of sea-level change observed at the NG tide gauge is not significantly affected by tectonic deformation, and that the proposed estimates at lines 1.–5. can be trusted, the results of Fig. 9 can be used to refine previous estimates of $\langle r^{GIS} \rangle$. In particular, they suggest that $\langle r^{GIS} \rangle$ could be somewhat biased toward positive values. The bias appears to be larger for the estimates by Rignot et al. (2008) and Slangen (2012) compared with the AR4 assessment. Because of Eq. (18), this produces exceedingly negative values of the local sea-level trend at NG, which prevent a full agreement with the observed rate of sea-level change. A disagreement at the ~1 mm yr^{-1} level between MOD and OBS, suggested by Fig. 9, would imply, according to Eq. (18), a reduction of ~0.2 mm yr^{-1} in $\langle r^{GIS} \rangle$. Hence, estimates (16) and (17) would be consistent with the GIS being almost in balance during the period 1961–2003 (i.e. $\langle r^{GIS} \rangle \approx 0$), which would match the AR4 assessment (15).

5. Conclusions

Despite the unsatisfactory state of Greenland tide gauges, we have shown that at least one of the available instrumental sea-level records (NG) can be of interest from a geophysical standpoint. The location of the NG station and its record length (~4 decades) makes it potentially useful for constraining volume changes in the GIS during a period (1958–2002) when only a few mass balance estimates exist for the GIS, sometimes characterized by a considerable degree of uncertainty. Our main results can be summarized in three points.

i) Analysis of the NG sea-level time series by standard regression methods clearly shows a linear sea-level rise and a negligible sea-level acceleration. The EEMD analysis of the NG record reveals a marked cyclic component with a period of ~18 years, probably representing the effect of the nodal tide. Based on previous AR4 assessments, results from the literature and on the sea-level fingerprint method, all sea-level components have been evaluated, along with their uncertainties. The methods employed can also be extended to all polar tide gauge records of adequate length.

ii) During period 1961–2003, GIA and the isostatic disequilibrium associated with melting of the GIS have been the dominating causes of sea-level variation at the NG tide gauge, but these processes have been acting in opposite directions: GIA has produced a sea-level rise, while the GIS has contributed a sea-level fall. When combined with the other sea-level contributions, including the steric component and various mass terms, the total modeled rate of sea-level change at NG is found to be broadly coherent with the observed trend, but its amplitude is not fully explained.

iii) In view of the large uncertainties in the modeled components of sea-level change at NG, the misfit between predictions and observations cannot be interpreted unambiguously. Nevertheless, two meaningful interpretations are possible. First, the NG tide gauge could be subject to a regional tectonic subsidence, at a level of 0.5–1 mm yr^{-1}. However, in view of the tectonic setting and the low rate of seismicity in SW Greenland, this relatively large subsidence rate appears unrealistic. As an alternative, the evidence from NG could indicate that the mass balance of the GIS was, during 1961–2003, closer to balance than suggested by several estimates in the literature that followed the AR4 assessment.

Acknowledgments

We are grateful to Kevin Fleming and to an anonymous reviewer for very constructive suggestions, to Florence Colleoni for helpful discussions, to Aimee Slangen for providing the gridded data for the terrestrial component of sea-level rise in the period 1961–2003 shown in Fig. 7, and to Luigi Bergamini for the technical assistance. We thank William Richard Peltier for making available the ICE-5G(VM2) GIA predictions and Kurt Lambeck for providing the chronology of the ice sheet model referred to as KL05 in the body of the paper. All figures have been drawn using GMT (Wessel and Smith, 1998). The sea-level fingerprints in Figs. 5 and 8 have been obtained by an improved version of the program SELEN, available from the Computational Infrastructure for Geodynamics (CIG), at the address: http://www.geodynamics.org/. This work has been partly funded by a DiSBeF (Dipartimento di Scienze di Base e Fondamenti, Urbino University) research grant.

References

Alley, R., Andrews, J., Brigham-Grette, J., Clarke, G., Cuffey, K., Fitzpatrick, J., Funder, S., Marshall, S., Miller, G., Mitrovica, J., Muhs, D., Otto-Bliesner, B., Polyak, L., White, J., 2010. History of the Greenland ice sheet: paleoclimatic insights. Quat. Sci. Rev. 29, 1728–1756.

Antonov, J., Levitus, S., Boyer, T., 2005. Steric variability of the world ocean, 1955–2003. Geophys. Res. Lett. 32 (12), L12602.

Bamber, J., Griggs, J., Hurkmans, R., Dowdeswell, J., Gogineni, S., Howat, I., Mouginot, J., Paden, J., Palmer, S., Rignot, E., Steinhage, D., 2013. A new bed elevation dataset for Greenland. Cryosphere 7, 499–510.

Barlow, N.L.M, Shennan, I., Long, A.J, Gehrels, W.R, Shaer, M.H, Woodroffe, S.A, Hillier, C., 2013. Salt marshes as late Holocene tide gauges. Global Planet. Chang. 106, 90–110 (http://www.sciencedirect.com/science/article/pii/S0921818113000738).

Barnhart, L., 2011. The Hilbert–Huang Transform: Theory, Applications, Development. (Ph.D. thesis) University of Iowa, U.S.A.

Bindoff, N., Willebrand, J., Artale, V., Cazenave, A., Gregory, J., Gulev, S., Hanawa, K., Le Quèrè, C., Levitus, S., Nojiri, Y., Shum, C., Talley, L.D., 2007. Observations: oceanic climate change and sea level. In: Solomon, S., Qin, D., Manning, M., Chen, Z., Marquis, M., Averyt, K., Tignor, M., Miller, H. (Eds.), Climate Change 2007: The Physical Science Basis, Intergovernmental Panel on Climate Change. Cambridge University Press, Cambridge, pp. 385–432.

Breaker, L.C., Ruzmaikin, A., 2013. Estimating rates of acceleration based on the 157-year record of sea level from San Francisco, California, U.S.A. J. Coast. Res. 29 (1), 43–51.

Cazenave, A., Remy, F., 2011. Sea level and climate: measurements and causes of changes. WIREs Clim. Chang. 2, 647–662.

Chao, B.F., Wu, Y.H., Li, Y.S., 2008. Impact of artificial reservoir water impoundment on global sea level. Science 320, 212–214.

Chung, W.Y., 2002. Earthquakes along the passive margin of Greenland: evidence of postglacial rebound control. Pageoph 159, 2567–2584.

Chung, W.Y., Gao, H., 1997. The Greenland earthquake of 11 July 1987 and postglacial reactivation along a passive margin. Bull. Seismol. Soc. Am. 87, 1058–1068.

De Boor, C., 1978. A practical guide to splines. Applied Mathematical Sciences, volume 27. Springer–Verlag, New York.

Douglas, B., 1991. Global sea level rise. J. Geophys. Res. 96, 6981–6992.

Douglas, B., 1997. Global sea-level rise: a redetermination. Surv. Geophys. 18, 279–292.

Dyurgerov, M.B., Meier, M.F., 2005. Glaciers and the changing earth system: a 2004 snapshot. Technical Report Occas. Pap. n. 58. Tech. Rep. Inst. of Arct. and Alp. Res. Univ. of Colorado, Boulder.

Ettema, J., van den Broeke, M., van Meijgaard, E., van de Berg, W., Bamber, J., Box, J., Bales, R., 2009. Higher surface mass balance of the Greenland ice sheet revealed by high-resolution climate modeling. Geophys. Res. Lett. 36, 12.

Farrell, W., Clark, J., 1976. On postglacial sea-level. Geophys. J. R. Astron. Soc. 46 (3), 647–667.
Fleming, K., Lambeck, K., 2004. Constraints on the Greenland ice sheet since the last glacial maximum from sea-level observations and glacial-rebound models. Quat. Sci. Rev. 23 (9–10), 1053–1077.
Fleming, K., Wünsch, J., Lambeck, K., 2009. Glacial-isostatic contributions to present-day sea-level change around Greenland. Technical Report STR05/09. GeoForschungsZentrum - Potsdam Department 1 Geodesy and Remote Sensing, Potsdam, Germany (Available at http://bib.gfz-potsdam.de/pub/str0509/0509.htm).
Gutenberg, B., 1941. Changes in sea level, postglacial uplift and mobility of the Earth's interior. Bull. Geol. Soc. Am. 52, 721–772.
Hanna, E., Huybrechts, P., Janssens, I., Cappelen, J., Steffen, K., Stephens, A., 2005. Runoff and mass balance of the Greenland ice sheet: 1958–2003. J. Geophys. Res. 110, D13108.
Henry, O., Prandi, P., Lovel, W., Cazenave, A., Jevrejeva, S., Stammer, D., Meyssignac, B., Koldunov, N., 2011. Tide gauge–based sea level variations since 1950 along the Norwegian and Russian coasts of the Arctic Ocean: contribution of the steric and mass components. J. Geophys. Res. 117 (C6), 1978–2012 (http://onlinelibrary.wiley.com/doi/10.1029/2011JC007706/abstrac).
Holgate, S.J., Matthews, A., Woodworth, P.L., Rickards, L.J., Tamisiea, M.E., Bradshaw, E., Foden, P.R., Gordon, K.M., Jevrejeva, S., Pugh, J., 2012. New data systems and products at the permanent service for mean sea level. J. Coast. Res. 29, 493–504.
Huang, N.E., Shen, Z., Long, S.R., Wu, M.C., Shih, H.H., Zheng, Q., Yen, N.C., Tung, C.C., Liu, H. H., 1998. The empirical mode decomposition and the Hilbert spectrum for nonlinear and non-stationary time series analysis. Proc. R. Soc. Lond. A Math. Phys. Eng. Sci. 454, 903–995.
Ishii, M., Kimoto, M., Sakamoto, K., Iwasaki, S., 2006. Steric sea level changes estimated from historical ocean subsurface temperature and salinity analyses. J. Oceanogr. 62 (2), 155–170.
Johnston, A., 1987. Suppression of earthquakes by large continental ice sheets. Nature 330, 467–469.
Lambeck, K., Smither, C., Johnston, P., 1998. Sea-level change, glacial rebound and mantle viscosity for northern Europe. Geophys. J. Int. 134, 102–144.
Landerer, F., Jungclaus, J., Marotzke, J., 2007. Ocean bottom pressure changes lead to a decreasing length-of-day in a warming climate. Geophys. Res. Lett. 34, L06307.
Meier, M., 1984. Contribution of small glaciers to global sea level. Science 226, 1418–1421.
Milne, G., Mitrovica, J., 1998. Postglacial sea-level change on a rotating Earth. Geophys. J. Int. 133, 1–10.
Milne, G.A., Gehrels, R.W., Hughes, C.W., Tamisiea, M., 2009. Identifying the causes of sea-level change. Nat. Geosci. 2, 471–478.
Mitrovica, J., Tamisiea, M.E., Davis, J.L., Milne, G., 2001. Recent mass balance of polar ice sheets inferred from patterns of global sea-level change. Nature 409, 1026–1029.
Olivieri, M., Spada, G., Antonioli, A., Galassi, G., 2014. Mazara del Vallo tide gauge observations (1906–1916): land subsidence or sea level rise? J. Coast. Res. (in press).
Peltier, W., 2004. Global glacial isostasy and the surface of the Ice-Age Earth: the ICE-5G(VM2) model and GRACE. Ann. Rev. Earth Planet. Sci. 32, 111–149.
Plag, H.P., 2000. Arctic tide gauges: a status report. Intergovernmental Oceanographic Commission of UNESCO.
Qingjie, Z., Huayong, Z., Lincheng, S., 2010. A new method for mitigation of end effect in empirical mode decomposition. Informatics in Control, Automation and Robotics (CAR), 2010 2nd International Asia Conference on, IEEE, pp. 400–403.
Rignot, E., Box, J., Burgess, E., Hanna, E., 2008. Mass balance of the Greenland ice sheet from 1958 to 2007. Geophys. Res. Lett. 35, L20502.
Rignot, E., Velicogna, I., van den Broeke, M., Monaghan, A., Lenaerts, J., 2011. Acceleration of the contribution of the Greenland and Antarctic ice sheets to sea level rise. Geophys. Res. Lett. 38, L05503.
Slangen, A., 2012. Modelling regional sea-level changes in recent past and future. (Ph.D. thesis) Utrecht University, the Netherlands.
Sørensen, L., Simonsen, S., Nielsen, K., Lucas-Picher, P., Spada, G., Adalgeirsdottir, G., Forsberg, R., Hvidberg, C., 2011. Mass balance of the Greenland ice sheet — a study of ICESat data, surface density and firn compaction modelling. Cryosphere 5, 173–186.
Spada, G., Galassi, G., 2012. New estimates of secular sea-level rise from tide gauge data and GIA modeling. Geophys. J. Int. 191 (3), 1067–1094.
Spada, G., Stocchi, P., 2007. SELEN: a Fortran 90 program for solving the "Sea Level Equation". Comput. Geosci. 33, 538–562.
Spada, G., Ruggieri, G., Sørensen, L., Nielsen, K., Melini, D., Colleoni, F., 2012. Greenland uplift and regional sea level changes from ICESat observations and GIA modelling. Geophys. J. Int. 189, 1457–1474.
Tamisiea, M., Mitrovica, J., Milne, G., Davis, J., 2011. Global geoid and sea level changes due to present-day ice mass fluctuations. J. Geophys. Res. 106 (B12), 30,849–30,863.
Tanaka, Y., Klemann, V., Martinec, Z., Riva, R.E.M., 2011. Spectral-finite element approach to viscoelastic relaxation in a spherical compressible Earth: application to GIA modelling. Geophys. J. Int. 184, 220–234.
Taylor, J.R., 1997. An introduction to error analysis: the study of uncertainties in physical measurements. University Science Books.
Torres, M.E., Colominas, M.A., Schlotthauer, G., Flandrin, P., 2011. A complete ensemble empirical mode decomposition with adaptive noise. Acoustics, Speech and Signal Processing (ICASSP), 2011 IEEE International Conference on, IEEE, pp. 4144–4147.
Trupin, A., Wahr, J., 1990. Spectroscopic analysis of global tide gauge sea level data. Geophys. J. Int. 100 (3), 441–453.
Turcotte, D.L., Schubert, G., 2002. Geodynamics. Cambridge University Press, Cambridge.
Velicogna, I., 2009. Increasing rates of ice mass loss from the Greenland and Antarctic ice sheets revealed by GRACE. Geophys. Res. Lett. 36, L19503.
Wada, Y., van Beek, L., Chao, B., Wu, Y.H., Bierkens, M.F.P., 2012. Past and future contribution of global groundwater depletion to sea-level rise. Geophys. Res. Lett. 39, L09402.
Wahl, T., Haigh, I., Woodworth, P., Albrecht, F., Dillingh, D., Jensen, J., Nicholls, R., Weisse, R., Woppelmann, G., 2013. Observed mean sea level changes around the north sea coastline from 1800 to present. Earth-Sci. Rev. 124, 51–67.
Wessel, P., Smith, W.H.F., 1998. New, improved version of generic mapping tools released. Eos 79, 579.
Woodroffe, S., Long, A., 2009. Salt marshes as archives of recent relative sea-level change in West Greenland. Quat. Sci. Rev. 28, 1750–1761.
Woodworth, P.L., Player, R., 2003. The permanent service for mean sea level: an update to the 21st century. J. Coastal Res. 19, 287–295.
Wu, Z., Huang, N.E., 2009. Ensemble empirical mode decomposition: a noise-assisted data analysis method. Adv. Adapt. Data Anal. 1 (01), 1–41.